

A new GaN-based converter design for electric vehicle charging system

Snehalika¹, Ranjeeta Patel¹, Amruta Abhishek¹, Chinmoy Kumar Panigrahi¹, Ranjan Keshari Pati²

¹School of Electrical Engineering, Kalinga Institute of Industrial Technology (KIIT) Deemed to be University, Bhubaneswar, India

²Department of Electrical Engineering, Srinix College of Engineering, Balasore, India

Article Info

Article history:

Received Oct 3, 2023

Revised Mar 17, 2024

Accepted Apr 5, 2024

Keywords:

Dual active bridge

Electric vehicle

Gallium nitride

Isolated bidirectional DC-DC converter

Multi-port converter

Triple active bridge charging

ABSTRACT

The research work proposes a gallium nitride (GaN) based isolated bidirectional DC-DC (IBDC)-triple active bridge (TAB) based multi-port converter (MPC) for electric vehicle (EV) charging. The proposed GaN IBDC-TAB based MPC incorporates one input port (Port 1) and two output ports (Port 2 and Port 3) for charging, implying the use of fewer components compared to a conventional dual active bridge (DAB) charging system. The output ports can be operated individually in single active bridge (SAB), Dual active bridge (DAB), and TAB modes. A 12 kW GaN IBDC-TAB based MPC converter is designed for simulation study using LTspice XVII software. In the TAB mode of operation, output Port 2 designated for Level-1 (L-1) charging produces 1.5 kW, and output Port 3 designated for Level-2 (L-2) charging produces 10.6 kW. The maximum efficiency of 98.87% is obtained in simulation for the MPC converter in TAB mode. For experimental validation, a 0.91 kW prototype is presented with Port 1, Port 2, and Port 3 voltages as 230 V, 120 V, and 200 V respectively with the considered switching frequency of 100 kHz. The single-phase-shift control strategy is implemented for controlling the transmitted power in the proposed GaN IBDC-TAB converter.

This is an open access article under the [CC BY-SA](https://creativecommons.org/licenses/by-sa/4.0/) license.



Corresponding Author:

Chinmoy Kumar Panigrahi

School of Electrical Engineering

Kalinga Institute of Industrial Technology (KIIT) Deemed to be University

Bhubaneswar 751024, Balasore, India

Email: chinmoy.panigrahifel@kiit.ac.in

1. INTRODUCTION

The world is a foot towards green energy as due to severe climate change, pollution, and health hazards making electric vehicles (EVs) a clear choice over the traditional internal combustion (IC) engines. The increased demand for EVs has led to the requirement for efficient and reliable EV charging systems [1]-[3]. A DC-DC converter can allow both unidirectional and bidirectional charging as per requirement. Bidirectional charging allows charging from the grid-to-vehicle (G2V) and vehicle-to-grid (V2G), as required [4].

The isolated bidirectional DC-DC converter (IBDC) is popular for EV charging applications [5]-[7]. The dual active bridge (DAB) offers bewitching attributes such as bidirectional capability of power transfer, soft-switching, high power transfer, and symmetric structure. The DAB topology-based converter can also operate in single active bridge (SAB) mode with an active input bridge and inactive output bridge [8], [9]. The power transfer to the output bridge happens through the natural conduction of the anti-parallel diodes reducing the complexity making it suitable for low-power applications where bidirectional power flow is not

required. However, the converter's efficiency is lower compared to DAB mode since only one active bridge is used. A TAB DC-DC converter is an IBDC with three active bridges resulting in higher efficiency and reduced switches as compared to conventional DAB based chargers. The TAB can also operate in SAB and DAB mode depending on the specific requirements of the EV charging application, such as power level, efficiency, cost, and control complexity [10]. Recent studies have documented the advantages of multi-port topology such as triple active bridge for EV charging, including improved scalability, higher power density, cost-effectiveness, reduced space requirements, improved user experience, and increased utilization [11]-[14].

EV battery chargers are categorized based on their power levels/rating, such as Level-1 (L-1), Level-2 (L-2), and Level-3 (L-3) [15], [16]. L-1 EV charging systems use a standard household 120V AC outlet and typically provide a charging power of 1.4 kW (low power rating vehicles). L-2 EV charging systems use a 240V AC power supply and typically provide a charging power of 3.3 kW to 19.2 kW (medium power rating vehicles). L-3 EV charging systems, also known as DC fast charging, use a high-power DC supply and can provide a charging power of up to 350 kW (high-power rating vehicles) [17].

The wide bandgap semiconductor material, gallium nitride (GaN) offers superior characteristics resulting in enhanced efficiency of the DC-DC converters for EV charging applications [18]. GaN devices have lower on-resistance and lower switching losses compared to traditional Si-based devices [19]-[21]. Among the available literature for control strategies proposed for controlling the transmitted power in the IBDC based TAB topology, the single-phase-shift (SPS) control technique has been chosen given its simplicity of operation [22]-[24].

In this paper, a GaN IBDC-TAB based multi-port converter (MPC) for EV charging application has been proposed. The simulations were carried out in LT spice XVII software to validate the functionality of the proposed GaN IBDC-TAB based MPC. Power levels of 1.5 kW and 10.6 kW in alignment with the L-1 and L-2 EV charging systems is obtained. Subsequently, a scaled-down prototype design of the proposed GaN IBDC-TAB based MPC converter is presented for EV charging system to validate the efficacy of the proposed model. The prototype model is designed for 0.906 kW with Port 2 as 0.192 kW and Port 3 as 0.714 kW, respectively. The power transmission in the GaN IBDC-TAB-based MPC converter is controlled by the SPS control strategy. The detailed research work is arranged as: i) Section 2 presents the proposed GaN IBDC-TAB based MPC converter along with its operation and design parameters; ii) Section 3 showcases the simulation results and experimental validation of the results; and iii) Section 4 concludes the paper.

2. PROPOSED GaN IBDC-TAB BASED MPC

Here, the IBDC-TAB based MPC is presented and discussed in detail. The IBDC-TAB converter incorporates a high-frequency transformer (HFT), which not only provides galvanic isolation but also regulates the power distribution to the output ports [25]. The key contributions of the proposed GaN IBDC-TAB based MPC are: i) multi-port charging, ii) high power operation, iii) high efficiency, iv) requirement of lesser components, v) lower switching losses, and vi) active bridge operation flexibility.

The proposed GaN IBDC-TAB based MPC converter is illustrated in Figure 1. The converter comprises three active ports interconnected through a three-winding high-frequency transformer (HFT). An input DC-link voltage, V_{in} and input DC-link current, I_{in} powers the input port through Port 1. The other two ports, Port 2 and Port 3 form output ports which are specifically designed to provide power for L-1 and L-2 EV charging respectively. All the ports of the GaN IBDC-TAB based MPC converter are equipped with four GaN devices, four anti-parallel diodes, and four snubber capacitors as presented in Figure 1. Furthermore, Port 2 and Port 3 are equipped with two series inductors, L_{s2} and L_{s3} , respectively. N_1 , N_2 , and N_3 are the number of turns on primary, secondary, and tertiary winding respectively of the HFT. The voltage denoted at primary, secondary and tertiary winding are V_{py} , V_{sy1} , and V_{sy2} , respectively. The currents flowing in L_{s2} and L_{s3} are denoted as I_{Ls2} and I_{Ls3} respectively. The output port voltages are V_{o1} , V_{o2} , and output port currents are I_{o1} , I_{o2} , respectively.

The entire operation of the proposed converter can be bifurcated into four modes and presented in Figure 2. The four modes indicating the status of active switches are presented as mode I in Figure 2(a), mode II in Figure 2(b), mode III in Figure 2(c), and mode IV in Figure 2(d). The port-wise operation for switches S1-S12 is tabulated in Table 1.

The SPS control strategy is utilized for controlling the transmitted power in GaN IBDC-TAB based MPC. Here, the bridges are made to operate at a 50% duty cycle with a fixed switching frequency. The power flow from input to output ports is controlled by varying the phase-shift value from a range of 0 to 0.5 radian (90°). The phase-shift, d is introduced between the input and output bridges of the HFT as indicated in Figure 3. The output and input voltages of the three-winding HFT are V_{py} , V_{sy1} , and V_{sy2} indicated in Figure 3. By referring Figure 3, buck mode of operation is evident with the same phase shift value applied to V_{sy1} , and

V_{sy2} concerning V_{py} , enabling G2V power flow. With positive and negative values of d , power flow modes of G2V and V2G respectively can be achieved.

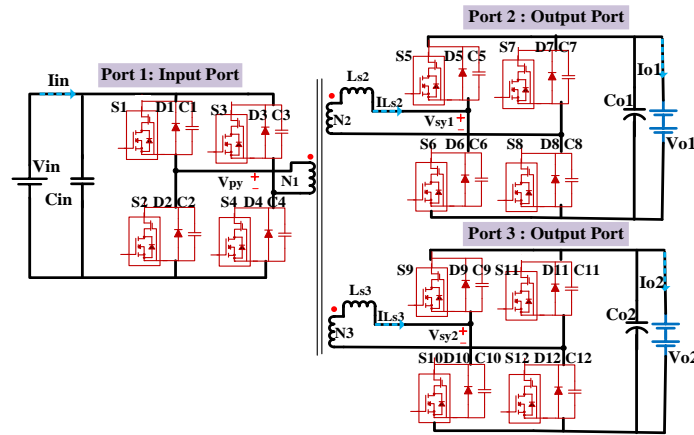


Figure 1. Circuit diagram of GaN IBDC-TAB based MPC converter

2.1. Principle of operation of TAB

The values of series inductor current at origin and at a value of d can be given by values $I_{(0)}$, and $I_{(d)}$ computed in (1) and (2). Where T_S is the time period, N_x stands for no. of turns, L_{S_x} stands for series inductor values, and V_{ox} stands for output voltage for the ports Port 2 and Port 3 respectively. Solving (1) and (2), the output current, I_{ox} of output ports, is computed using (3). It can be seen that I_{ox} depends directly on the values of phase-shift, and turns-ratio and indirectly on the value of series inductance [11], [25]. The proposed GaN IBDC-TAB based MPC converter is designed for a unity voltage gain, g for both the output ports. The value of g for both the output ports can be given by (4). The unity gain protects the converter, in low-load conditions reducing the voltage stress on the switches and HFT [25].

$$I_{(0)} = T_S \cdot \frac{[N \cdot V_{in} + (2d-1)V_o]}{4L_S} \quad (1)$$

$$I_{(d)} = T_S \cdot \frac{[N \cdot V_{in} \cdot (2d-1) + V_o]}{4L_S} \quad (2)$$

$$I_{ox} = \frac{N \cdot V_{in} \cdot (d-d^2)}{2L_S \cdot f} \quad (3)$$

$$g_x = \frac{V_{ox}}{N_x \cdot V_{in}} \quad (4)$$

2.2. ZVS operation

The IBDC-TAB converter's inherent soft-switching capability is discussed in this section. To achieve zero voltage switching (ZVS) in the output ports, the ZVS conditions defined in (5) need to be fulfilled for the inductor current, $I_{(d)}$ [25]. Solving for the above inequality in (5), the (6) determines the phase-shift value at which ZVS occurs for both the output ports.

$$\frac{T_S \cdot [N_x \cdot V_{in} \cdot (2d-1) + V_{ox}]}{4L_{S_x}} \geq 0 \quad (5)$$

$$d \geq 0.5 - \frac{V_{ox}}{N_x \cdot V_{in}} \quad (6)$$

Where the value of f_x represents the parameter values concerned for both the output ports for (1) to (6). On deviating from the unity value of g , the ZVS operation of the converter is limited [25]. The eight GaN devices in the IBDC-TAB converter are switched OFF under ZVS conditions. The anti-parallel diodes and the snubber capacitors associated with each GaN switch play a crucial role in achieving the ZVS condition for all the ports of GaN IBDC-TAB MPC.

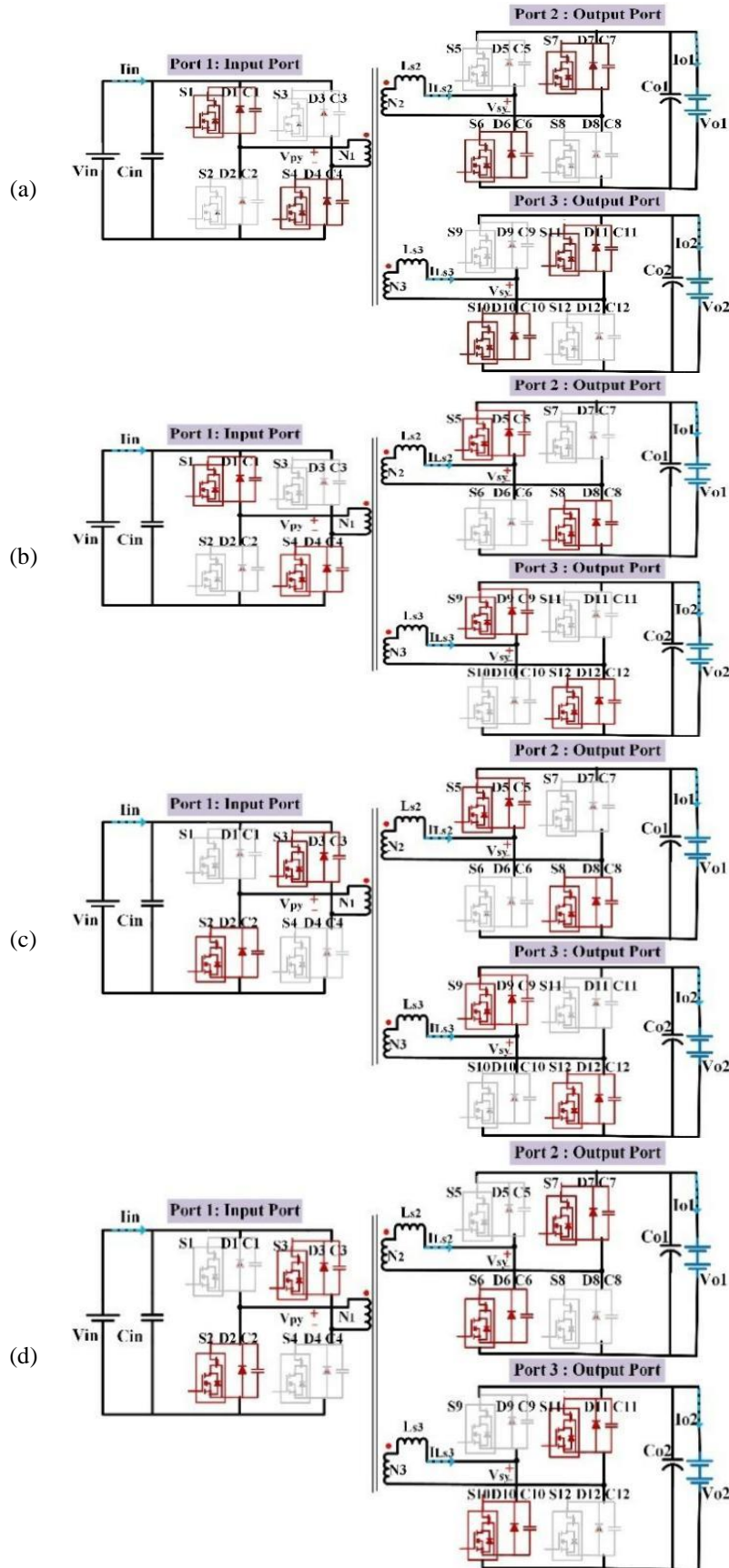


Figure 2. Four modes of operation of the GaN IBDC-TAB-based MPC converter: (a) mode I, (b) mode II, (c) mode III, and (d) mode IV

Table 1. Operation of converter in TAB mode

Mode	Active Ports		
	Port 1	Port 2	Port 3
I	S1, S4	S6, S7	S10, S11
II	S1, S4	S5, S8	S9, S12
III	S2, S3	S5, S8	S9, S12
IV	S2, S3	S6, S7	S10, S11

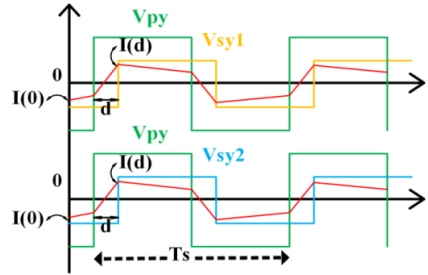


Figure 3. Voltage and current waveform of the DAB topology for Port 2 and Port 3

2.3. Parameter design of GaN IBDC-TAB based MPC

The primary aim of the research paper is to develop a prototype model for the GaN IBDC-TAB based MPC designed for EV charging applications. The simulation analysis is carried out using the LTspice XVII software tool for the GaN IBDC-TAB based MPC converter. The entire design is based on the utilization of twelve GaN devices for all three ports. The obtained power levels at both the output ports are on par with the power requirements for L-1 and L-2EV charging.

2.3.1. Three-winding HFT turns ratio

The turns ratio of HFT is calculated using (7). The value of N_1 is considered unity for a simplified calculation. The ratio N_2/N_1 and N_3/N_1 is calculated to be 0.33 and 0.4 respectively using (7) for simulation analysis. The voltage ratio, g can be controlled by varying the turns ratio, $\frac{N_2}{N_1}$ and $\frac{N_3}{N_1}$ of the HFT.

$$\frac{N_2}{N_1} = \frac{V_{o1}}{V_{in}}, \frac{N_3}{N_1} = \frac{V_{o2}}{V_{in}} \quad (7)$$

2.3.2. IBDC-TAB series inductor

Considering a phase-shift value of 0.5, the series inductor values of IBDC-TAB for Port 2 and Port 3 [11], are calculated using (8). The values of L_{s2} and L_{s3} are computed and listed in Table 2.

$$L_{sx} \geq \frac{N_x \cdot V_{in} \cdot T_s}{2 \cdot I_{ox}} (d - d^2) \quad (8)$$

The computed simulation parameters for the GaN IBDC-TAB based MPC are tabulated in Table 2 for a phase-shift value of 0.5 and at 100 kHz switching frequency.

Table 2. Circuit parameters of the MPC converter

Parameters	Symbol	Value
Input DC-link voltage	V_{in} (V)	540
Input current	I_{in} (A)	26.25
Port 2 in TAB mode	V_{o1} (V)	120.59
	I_{o1} (A)	12.54
	P_{o1} (W)	1512.2
Port 3 in TAB mode	V_{o2} (V)	206.19
	I_{o2} (A)	51.55
	P_{o2} (W)	10629.6
Total output power (W) ($P_{o1} + P_{o2}$)	P_o (W)	12141.2
Efficiency	η	95.79 %
Series inductor Port 2	L_{s2} (μ H)	17.38
Series inductor Port 3	L_{s3} (μ H)	9

The proposed GaN IBDC-TAB based MPC converter can also be operated in SAB and DAB as per the operational requirements providing active bridge operational flexibility. The four modes of operation in SAB mode are presented in Figures 4(a)-4(d) with switching pulses only being provided to the Port 1 switches, S1-S4 and diode conduction in Port 2 or Port 3. In DAB configuration, the four modes of operation are presented in Figures 5(a)-5(d) with switching pulses being provided to Port 1, Port 2, or Port 3. The output port, Port 2 is selected for representation of SAB and DAB operation. The different active bridge operational flexibility of GaN IBDC-TAB based MPC converter for both the SAB and DAB configuration is listed in Table 3.

Table 3. Operation of converter in SAB and DAB modes

Mode	SAB		DAB	
	Port 1	Port 2/ Port 3	Port 1	Port 2/ Port 3
I	S1, S4	D6, D7	S1, S4	S10, S11
II	S1, S4	D5, D8	S1, S4	S9, S12
III	S2, S3	D5, D8	S2, S3	S9, S12
IV	S2, S3	D6, D7	S2, S3	S10, S11

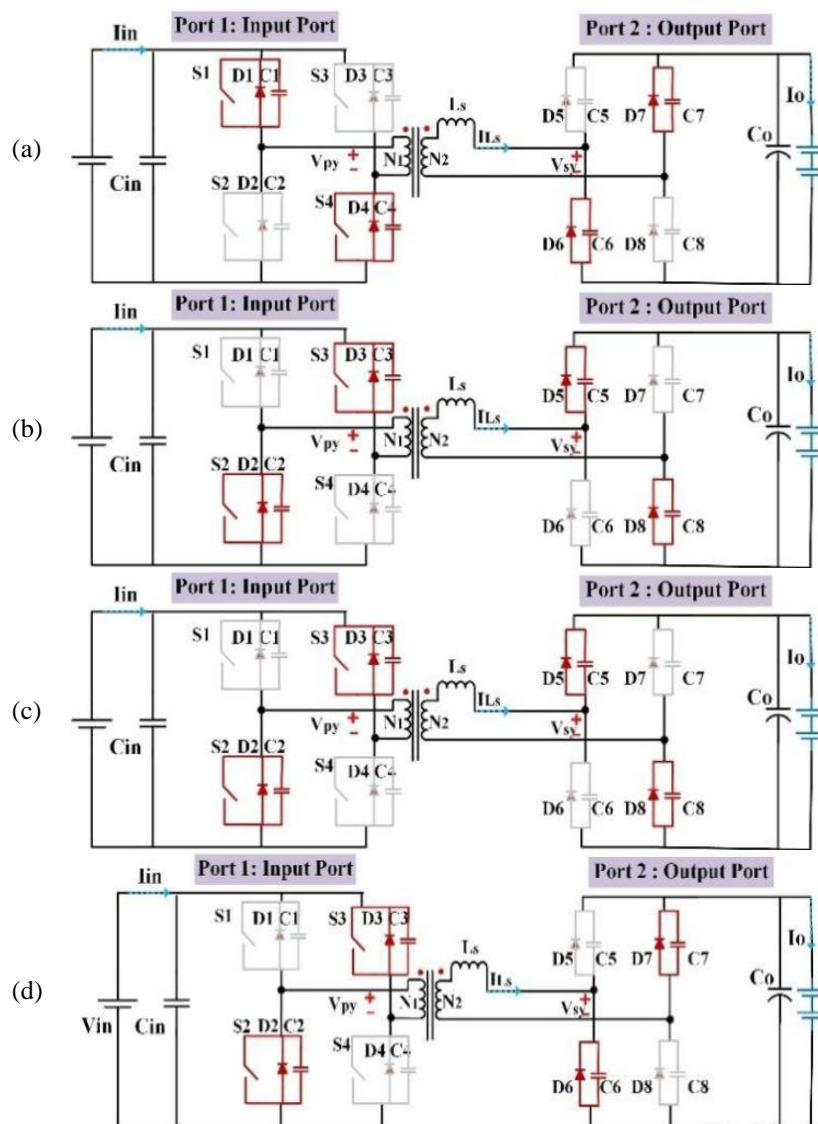


Figure 4. Four modes of operation of GaN IBDC-TAB in SAB mode: (a) mode I, (b) mode II, (c) mode III, and (d) mode IV

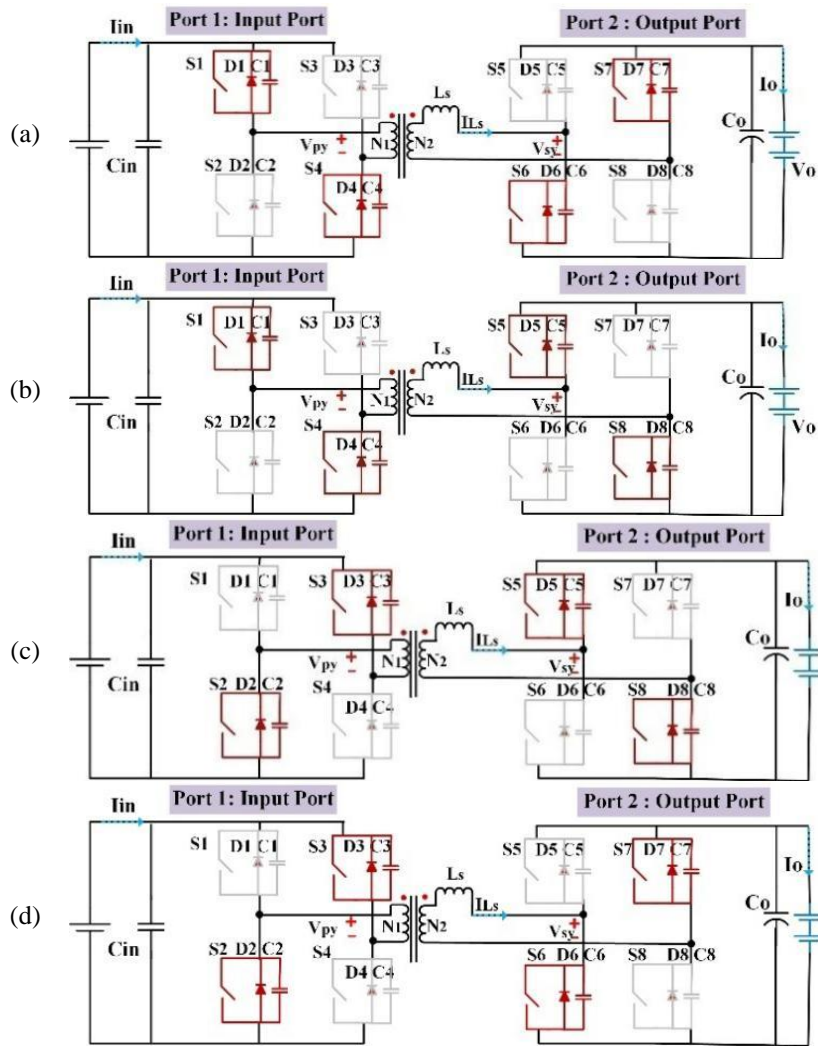


Figure 5. Four modes of operation of GaN IBDC-TAB in DAB mode: (a) mode I, (b) mode II, (c) mode III, and (d) mode IV

3. RESULTS AND DISCUSSION

3.1. Simulation results

To confirm the functionality of the proposed GaN IBDC-TAB based MPC, LTspice XVII simulation tool is utilized. Figures 6-8 show simulation results at 100 kHz switching frequency for the buck mode of operation of the GaN IBDC-TAB based MPC converter. Figure 6 presents the HFT voltages of primary, and secondary in the first plot. The second plot and third plot present the output parameters, V_{o1} , and I_{o1} of Port 2 and V_{o2} , and I_{o2} of Port 3 respectively. The output parameters, V_{o1} and I_{o1} for Port 2 in SAB operation are depicted in Figure 7. The output parameters V_{o2} and I_{o2} for Port 3 in DAB operation are presented in Figure 8.

The gate of the switches is driven with V_{GS} of 6 V. The value of gate drive voltage, switch voltage, switch current, current through the anti-parallel diode and snubber capacitor is plotted in Figures 9-11 respectively. The ZVS condition for switches S2 of Port 1, S6 of Port 2, and S10 of Port 3 for TAB operation can be determined from Figures 9-11, respectively.

The maximum efficiency of 98.86% is obtained with 11 kW output power. The efficiency vs output power is plotted in Figure 12. The converter is verified for phase-shift value, d varying from 0 to a maximum value of 0.5, and efficiency vs phase-shift is plotted in Figure 13 respectively. The output power versus phase-shift plot is plotted in Figure 14. The power achieved at Port 2 and Port 3 in TAB mode of operation is maximum with values of 1.5 kW and 10.6 kW, respectively at a phase-shift value of 0.389. The output voltage versus phase-shift plot for Port 2 and Port 3 is illustrated in Figure 15 for TAB mode of operation. Figure 15 indicates the increasing magnitude of output voltage with increasing values of phase-shift. Port 2 delivered a voltage of 179.48 V and Port 3 delivered a voltage of 215.4 V at a phase-shift of 0.389.

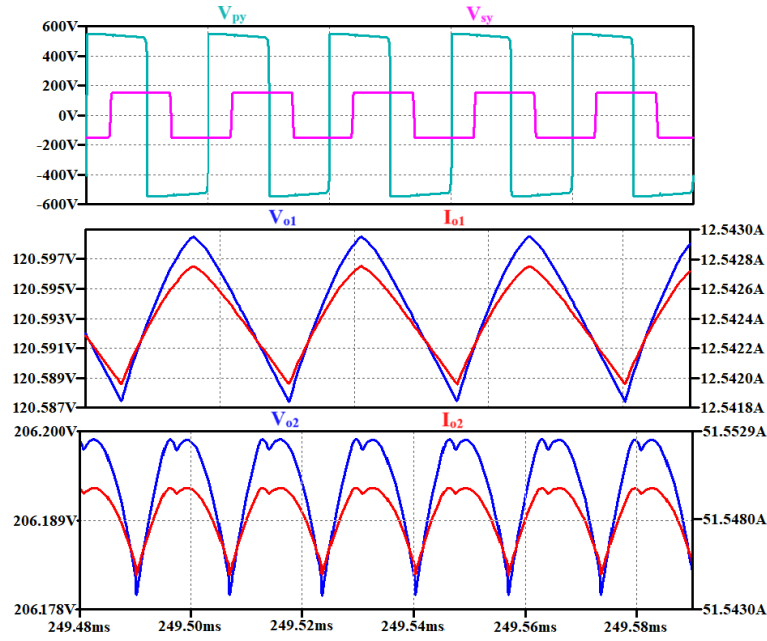


Figure 6. Output waveform in TAB: primary and secondary of HFT, V_{py} , and V_{sy1} (first plot), V_{o1} and I_{o1} (second plot), and V_{o2} , and I_{o2} (third plot)

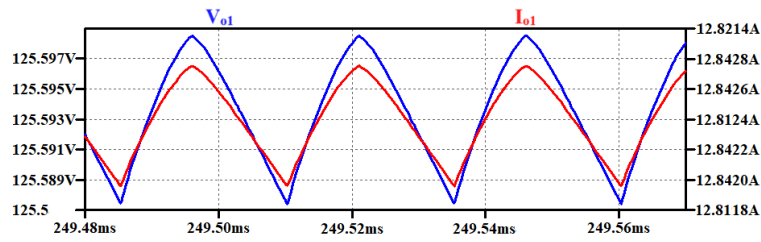


Figure 7. Output Port 2 waveform in SAB: V_{o1} and I_{o1}

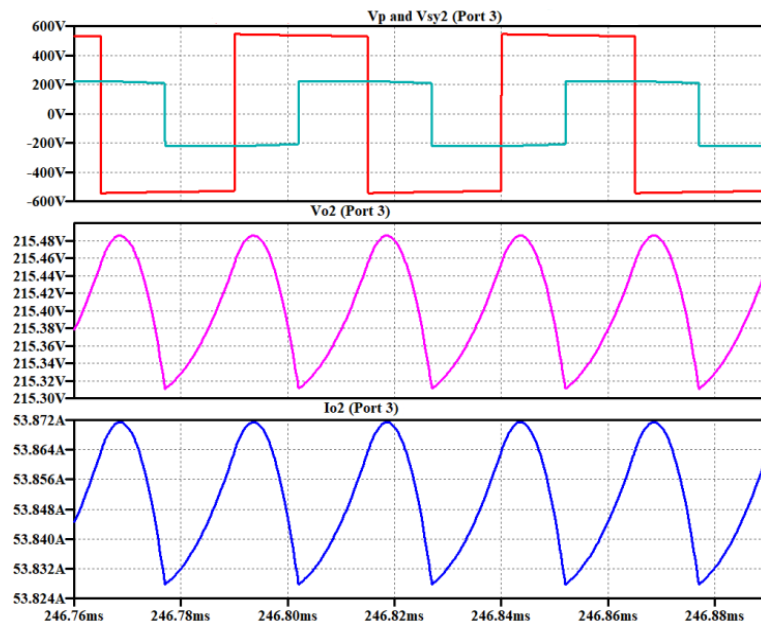


Figure 8. Output Port 3 waveform in DAB: primary and secondary of HFT, V_{py} , and V_{sy1} (first plot), V_{o2} (second plot), and I_{o2} (third plot)

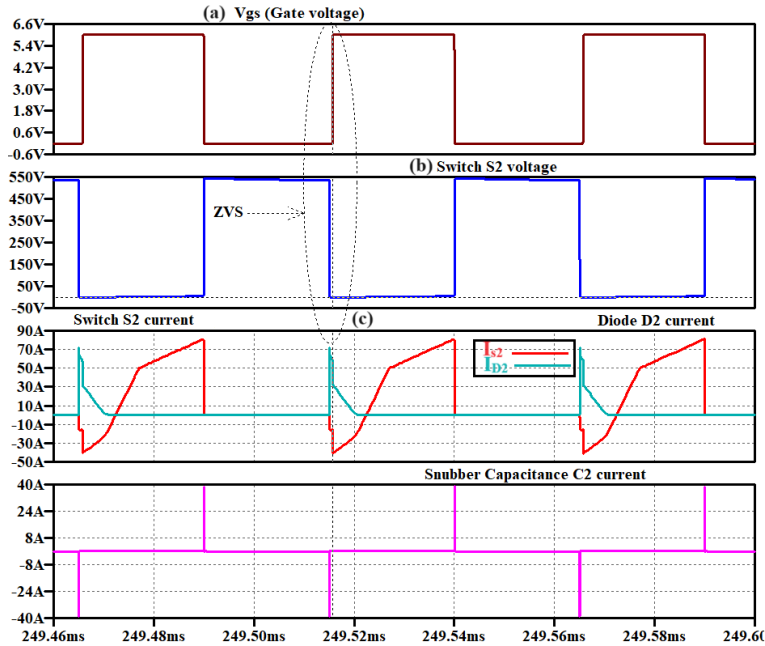


Figure 9. Parameters of switch S2 of Port 1

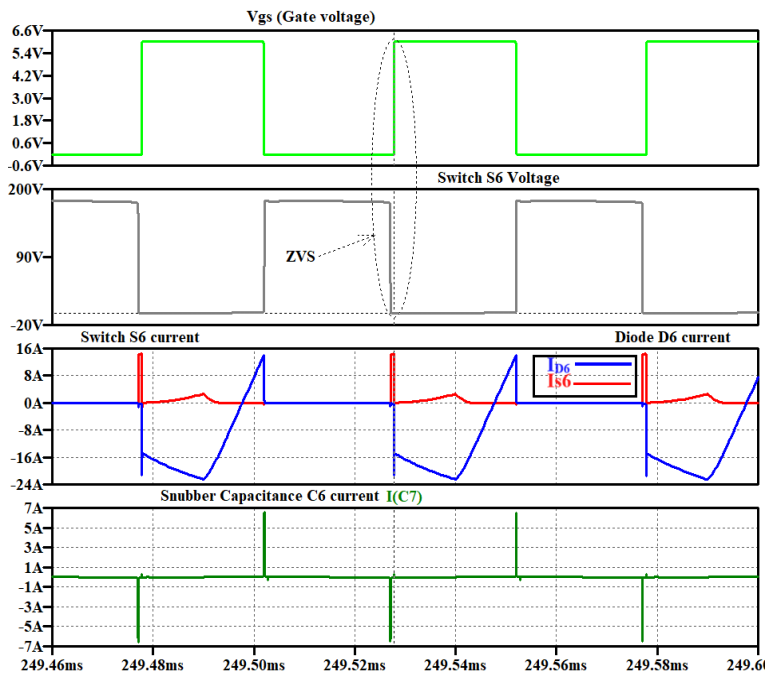


Figure 10. Parameters of switch S6 of Port 2

3.2. Experimental results

Using the proposed model, a prototype of a GaN IBDC-TAB based MPC converter has been designed to validate the functionality of the proposed converter in section 2. The GaN device-based converter illustrated in Figure 16 can transmit 0.906 kW of power operating at a switching frequency of 100 kHz. The GaN device selected for the IBDC-TAB based MPC converter is a 650 V GaN FET manufactured by Nexperia. The GaN device deployed in all the ports of the IBDC-TAB converter is presented in Figure 17 and its parameters are listed in Table 4. The GAN041-650WSB, utilized in the designed converter possesses minimal switching losses and has a very low on-state resistance.

The designed prototype of the converter can operate with an input voltage of up to 230 V and produce a maximum output voltage of 120 V and 200 V respectively at both the output ports. The converter's primary side is linked to a 3-phase rectifier and is allowed to operate at a maximum of 230 V for experimental purposes. The two output ports are linked to pre-charged capacitors of 120 V and 200 V with load resistors of 75 Ω and 56 Ω respectively for Port 2 and Port 3. The parameters of the converter are determined by utilizing (1) to (9) derived from the steady-state model as discussed in section 2. From (9), the series inductance values were calculated as 93 μH and 70 μH for the worst-case scenario of maximum power transfer. Table 5 presents the designed parameters of the prototype.

The turns-ratio of the HFT, $N_1:N_2:N_3$ for the prototype is designed as turns-ratio as 1:0.52:0.87. The output power obtained at Port 2 is 0.192 kW and at Port 3 is 0.714 kW. This resulted in 0.906 kW of total power from the GaN IBDC-TAB based MPC. Under these operating conditions, the efficiency of 95.83% is obtained at a phase-shift of 0.167. The phase-shift is chosen as 0.167 as per experimental limitations. The average output current flowing in Port 2 is 1.6 A and Port 3 is 3.57 A at a switching frequency of 100 kHz. The ripple in the output voltage of the converter is found to be less than 1%. The switching pulses for GaN devices S1-S12 are generated from a DSP processor TMS320F28379D. According to the manufacturer's datasheet, the switching time of GaN device is 28 nano seconds. Hence, a dead time of 53 nano seconds was introduced between the top and bottom switches of one leg in Port 1. The recorded 100 kHz PWM switching pulses for switches S1, S2, S3, and S4 of Port 1, S5, S6, S7, and S8 of output Port 2 and S9, S10, S11, and S12 of the output port, Port 3 are presented in Figures 18-20 respectively. Figure 21 represents the phase-shift of 0.167 introduced between switches S1, and S2 of Port 1 and switches bridge S9, and S10 of Port 3 of the GaN IBDC-TAB based MPC converter. The results obtained for the proposed converter in TAB mode are presented in Figures 22-24.

The same analysis has been extended for the SAB and DAB operation of the GaN IBDC-TAB based MPC. Figure 23 represents the parameters obtained at Port 2 in the SAB mode of operation. The results obtained show the voltages of V_{py} as 414 V peak-to-peak, and V_{sy1} as 240 V peak-to-peak, V_{o1} of 120 V and I_{o1} of 1.6 A at Port 2 with a resistive load of 75 Ω . Figure 24 represents the results in DAB mode of operation with voltage of V_{py} as 414 V peak-to-peak, V_{sy2} as 400 V peak-to-peak, V_{o2} of 200 V and I_{o2} of 3.57 A at Port 3 with a resistive load of 56 Ω . Figure 25 and Figure 26 represent the ZVS operation of the GaN IBDC-TAB based MPC converter. Figure 25 highlights the ZVS turn-off at switch S5 of Port 2 clearly indicating gate drive voltage V_{gs} , switch voltage, V_{ds} , and switch current, I_D . The switch S5 turns-off at zero value of V_{ds} that can clearly be seen in Figure 25. Figure 26 highlights the ZVS turn-off at switch S9 of Port 3 indicating plots of gate drive voltage V_{gs} , and switch voltage, V_{ds} . The switch S9 turns-off at zero value of V_{ds} as can be seen in Figure 26. The experimental results presented in Figure 25 and Figure 26 confirm the operation of the converter prototype over the ZVS condition and validate the GaN IBDC-TAB based MPC model presented in section 2.

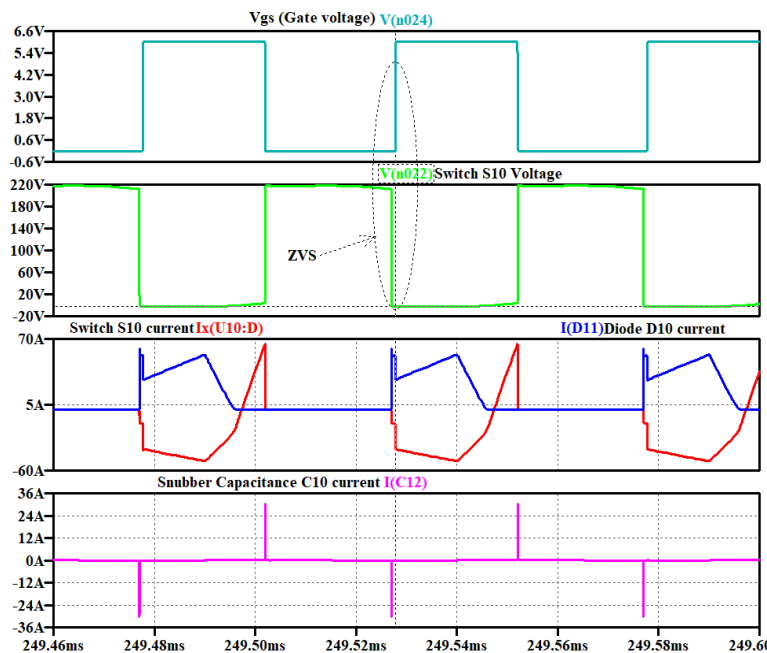


Figure 11. Parameters of switch S10 of Port 3

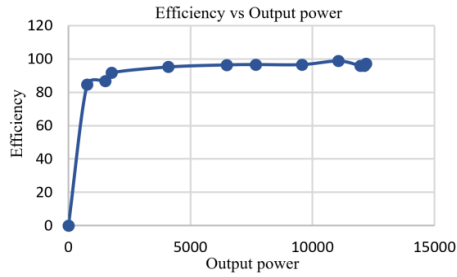


Figure 12. Efficiency vs overall output power (W)

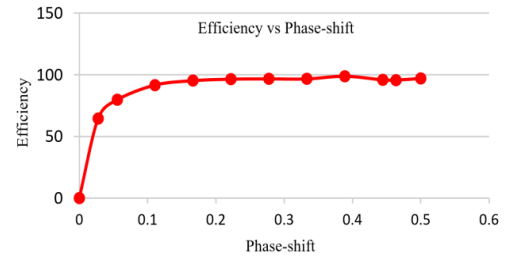


Figure 13. Efficiency vs phase-shift

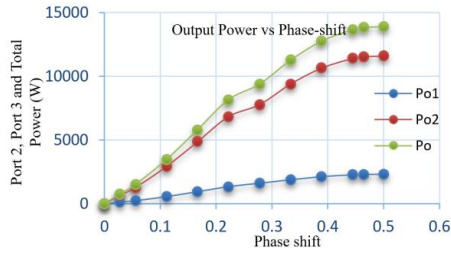


Figure 14. Phase-shift vs output power

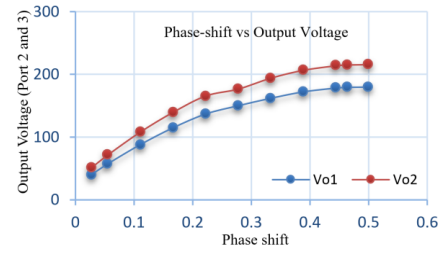


Figure 15. Output voltage at Port 2 and Port 3 vs phase-shift

Table 4. GaN device ratings

Device	GaN FET
Manufacturer	Nexperia
Part no.	GAN041-650WSB
V_{DS} (V)	650
$I_{DS(max)}$ (A)	47.2
$R_{DS(on)max}$ (m Ω)	41
Q_G (Gate charge) (nC)	6.6

Table 5. Experimental parameters of prototype

Parameters	Rating	Parameters	Rating
Input DC-link voltage (V)	230	Output power (kW) Port 2 and Port 3	0.192
Average input current (A)	4.35	Maximum power obtained (kW)	0.906
Phase-shift	0.167	Efficiency (%)	90.6
Output voltage (V) (avg) Port 2 and Port 3 in SAB, DAB and TAB modes	200	Leakage inductor (μ H) Port 2 and Port 3	93.6 and 70.5
Output current (A) (avg) Port 2 and Port 3	1.6	Snubber capacitor (nF) Port 1, Port 2, and Port 3	1
	3.571		

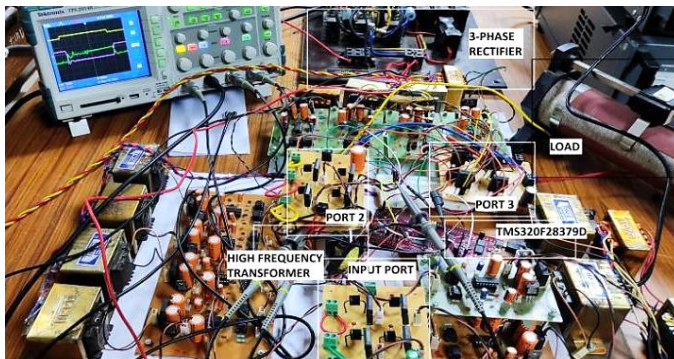


Figure 16. 0.906 kW prototype of IBDC-TAB based MPC converter

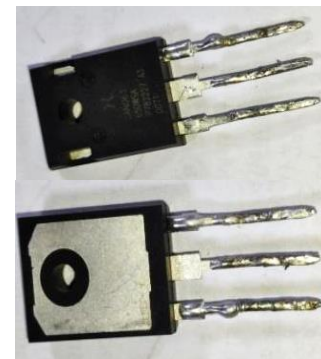


Figure 17. Front and back view of Nexperia 650 V, 35 m Ω gallium nitride (GaN) FET in a TO-247 package

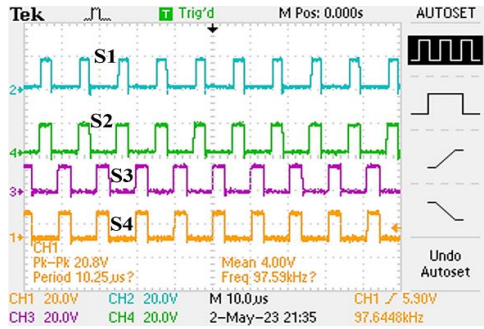


Figure 18. Switching pulses of 100 kHz for S1, S2, S3, and S4 of Port 1

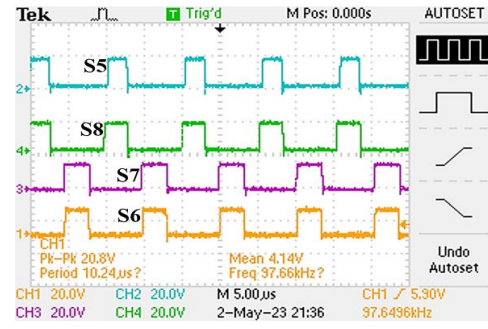


Figure 19. Switching pulses of 100 kHz for S5, S6, S7, and S8 of Port 2

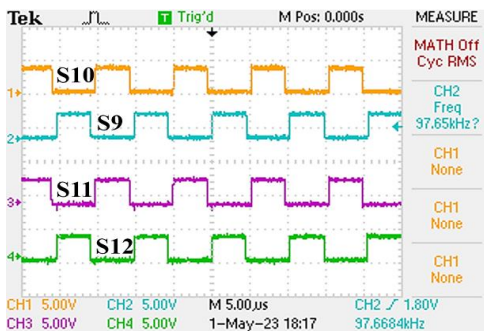


Figure 20. switching pulses of 100 kHz for S9, S10, S11, and S12 of Port 3

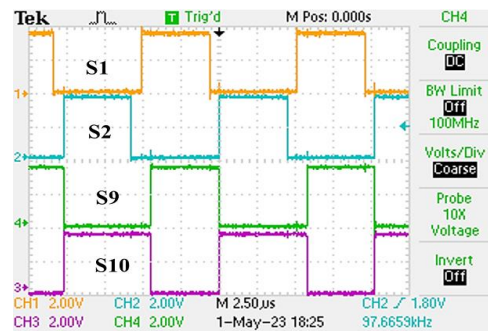


Figure 21. Phase-shift of 0.167 introduced between switches S1, and S2 of Port 1 and switches S9 and S10 of Port 3

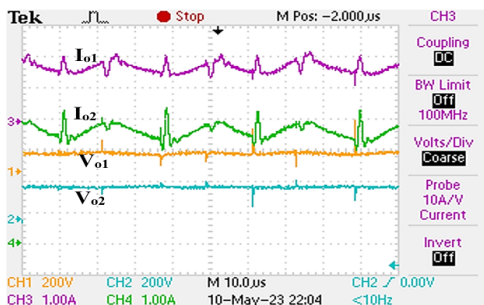


Figure 22. V_{o1} , and I_{o1} at Port 2 and V_{o2} , and I_{o2} at Port 3 respectively in TAB

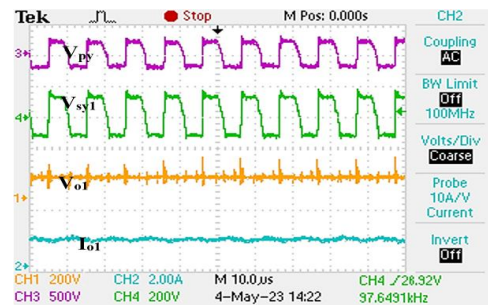


Figure 23. Voltages of HFT as V_{py} , and V_{sy1} , load voltage, V_{o1} and load current, I_{o1} in SAB at Port 2

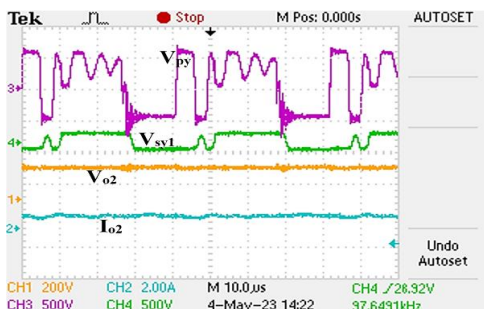


Figure 24. Voltages at primary and secondary of HFT as V_{py} , and V_{sy1} , V_{o2} , and I_{o2} in DAB at Port 3

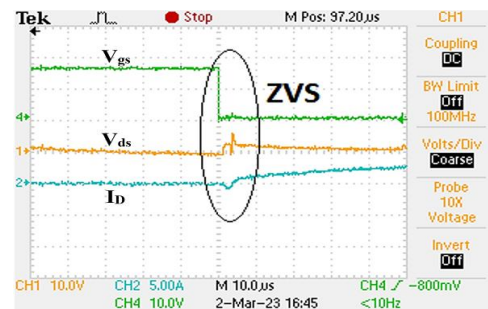


Figure 25. Port 2 switch S5 waveform at ZVS operation: gate drive voltage, V_{gs} , switch voltage, V_{ds} , and switch current, I_D

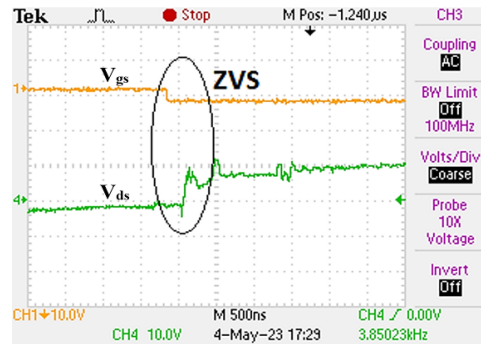


Figure 26. Port 3 switch S9 waveform at ZVS operation: gate drive voltage V_{gs} , and switch voltage, V_{ds}

4. CONCLUSION

The proposed GaN IBDC-TAB based MPC is designed for the G2V mode of operation with one common input port and two output ports to meet the charging requirements for L-1 and L-2 EV charging. The performance analysis for the proposed converter is studied both in simulation and experimental setup. The simulation study of the GaN IBDC-TAB based MPC converter is carried out using LTspice XVII simulation tool. The study focused on output parameters of voltage, current, and power. The designed 12 kW GaN IBDC-TAB based MPC converter can render 1.5 kW and 10.6 kW at Port 2 and Port 3 respectively. The converter in TAB mode of operation is able to achieve output voltage and current of values 179.48 V, 12.54 A, and 215.4 V, 51.54 A at Port 2 and Port 3 respectively. Operation of the proposed converter in SAB configuration and DAB configuration enhanced the versatility of the converter. The proposed GaN IBDC-TAB based MPC converter operating at 100 kHz obtained a maximum efficiency of 95.79 % at a phase-shift value of 0.389.

A prototype of 0.91 kW GaN IBDC-TAB based MPC converter is designed with an input DC-link voltage of 230 V and output voltage of 120 V at Port 2 and 200 V at Port 3 respectively. The PWM switching pulses of 100 kHz are provided by using a TMS320F28379D DSP processor. The maximum efficiency of 95.83% was recorded during experimental measurements with obtained output powers of 0.192 kW and 0.714 kW at Port 2 and Port 3 respectively. The beauty of the GaN IBDC-TAB based MPC converter is that it can operate in SAB, DAB, and TAB as operational requirements of EV charging applications. The multi-port structure allowed the converter to have fewer components in the EV charging system as compared to traditional EV charging systems. The ZVS operation is obtained both in simulation and experimental results minimizing the switching losses of the converter and improving the efficiency of the converter.





REFERENCES

- [1] K. Clement-Nyns, E. Haesen, and J. Driesen, "The impact of charging plug-in hybrid electric vehicles on a residential distribution grid," *IEEE Transactions on Power Systems*, vol. 25, no. 1, pp. 371–380, Feb. 2010, doi: 10.1109/TPWRS.2009.2036481.
- [2] W. A. Salah *et al.*, "Electric vehicle technology impacts on energy," *International Journal of Power Electronics and Drive Systems (IJPEDS)*, vol. 10, no. 1, p. 1, Mar. 2019, doi: 10.11591/ijpeds.v10.i1.pp1-9.
- [3] J. A. P. Lopes, F. J. Soares, and P. M. R. Almeida, "Integration of electric vehicles in the electric power system," *Proceedings of the IEEE*, vol. 99, no. 1, pp. 168–183, Jan. 2011, doi: 10.1109/JPROC.2010.2066250.
- [4] G. R. Chandra Mouli, M. Kefayati, R. Baldick, and P. Bauer, "Integrated PV charging of EV fleet based on energy prices, V2G, and offer of reserves," *IEEE Transactions on Smart Grid*, vol. 10, no. 2, pp. 1313–1325, Mar. 2019, doi: 10.1109/TSG.2017.2763683.
- [5] V. Karthikeyan and R. Gupta, "Multiple-input configuration of isolated bidirectional DC–DC converter for power flow control in combinational battery storage," *IEEE Transactions on Industrial Informatics*, vol. 14, no. 1, pp. 2–11, Jan. 2018, doi: 10.1109/TII.2017.2707106.
- [6] V. T. Tran, D. Sutanto, and K. M. Muttaqi, "The state of the art of battery charging infrastructure for electrical vehicles: Topologies, power control strategies, and future trend," in *2017 Australasian Universities Power Engineering Conference (AUPEC)*, Nov. 2017, pp. 1–6. doi: 10.1109/AUPEC.2017.8282421.
- [7] A. M. W. C. Bhuvaneshwari, S. M. Shyni, G. M. Sheeba, M. S. Mahendra, and V. Jaishree, "DC-DC converter based power management for go green applications," *International Journal of Power Electronics and Drive Systems (IJPEDS)*, vol. 10, no. 4, pp. 2046–2054, Dec. 2019, doi: 10.11591/ijpeds.v10.i4.pp2046-2054.
- [8] K. Bathala, D. Kishan, and N. Harischandrapa, "High frequency isolated bidirectional dual active bridge DC-DC converters and its application to distributed energy systems: an overview," *International Journal of Power Electronics and Drive Systems (IJPEDS)*, vol. 14, no. 2, pp. 969–991, Jun. 2023, doi: 10.11591/ijpeds.v14.i2.pp969-991.
- [9] M. N. Kheraluwala, R. W. Gascoigne, D. M. Divan, and E. D. Baumann, "Performance characterization of a high-power dual active bridge DC-to-DC converter," *IEEE Transactions on Industry Applications*, vol. 28, no. 6, pp. 1294–1301, 1992, doi: 10.1109/28.175280.





- [10] P. Purgat, S. Bandyopadhyay, Z. Qin, and P. Bauer, "Zero voltage switching criteria of triple active bridge converter," *IEEE Transactions on Power Electronics*, vol. 36, no. 5, pp. 5425–5439, May 2021, doi: 10.1109/TPEL.2020.3027785.
- [11] N. D. Dao, D.-C. Lee, and Q. D. Phan, "High-efficiency SiC-based isolated Three-Port DC/DC converters for hybrid charging stations," *IEEE Transactions on Power Electronics*, vol. 35, no. 10, pp. 10455–10465, Oct. 2020, doi: 10.1109/TPEL.2020.2975124.
- [12] A. K. Bhattacharjee, N. Kutkut, and I. Batarseh, "Review of multiport converters for solar and energy storage integration," *IEEE Transactions on Power Electronics*, vol. 34, no. 2, pp. 1431–1445, Feb. 2019, doi: 10.1109/TPEL.2018.2830788.
- [13] A. S. and S. K. R., "Review of multiport isolated bidirectional converter interfacing renewable and energy storage systems," *International Journal of Power Electronics and Drive System (IJPEDS)*, vol. 11, no. 1, pp. 466–476, 2020, doi: 10.11591/ijpeds.v11.i1.pp466-476.
- [14] H. Tao, A. Kotsopoulos, J. L. Duarte, and M. A. M. Hendrix, "Family of multiport bidirectional DC–DC converters," *IEE Proceedings - Electric Power Applications*, vol. 153, no. 3, pp. 451–458, 2006, doi: 10.1049/ip-epa:20050362.
- [15] A. Khaligh and M. D'Antonio, "Global trends in high-power on-board chargers for electric vehicles," *IEEE Transactions on Vehicular Technology*, vol. 68, no. 4, pp. 3306–3324, Apr. 2019, doi: 10.1109/TVT.2019.2897050.
- [16] J. Yuan, L. Dorn-Gomba, A. D. Callegaro, J. Reimers, and A. Emadi, "A review of bidirectional on-board chargers for electric vehicles," *IEEE Access*, vol. 9, pp. 51501–51518, 2021, doi: 10.1109/ACCESS.2021.3069448.
- [17] M. Yilmaz and P. T. Krein, "Review of battery charger topologies, charging power levels, and infrastructure for plug-in electric and hybrid vehicles," *IEEE Transactions on Power Electronics*, vol. 28, no. 5, pp. 2151–2169, May 2013, doi: 10.1109/TPEL.2012.2212917.
- [18] J. Millan, P. Godignon, X. Perpina, A. Perez-Tomas, and J. Rebollo, "A survey of wide bandgap power semiconductor devices," *IEEE Transactions on Power Electronics*, vol. 29, no. 5, pp. 2155–2163, May 2014, doi: 10.1109/TPEL.2013.2268900.
- [19] M. J. Carra, H. Tacc, and J. Lipovetzky, "Performance evaluation of GaN and Si based driver circuits for a SiC MOSFET power switch," *International Journal of Power Electronics and Drive Systems (IJPEDS)*, vol. 12, no. 3, p. 1293, Sep. 2021, doi: 10.11591/ijpeds.v12.i3.pp1293-1303.
- [20] Snehalika, R. Patel, C. K. Panigrahi, and A. K. Rathore, "High-power isolated bidirectional Three-port DC-DC converter for Level-1 and Level-2 charging," in *2022 IEEE 2nd International Conference on Sustainable Energy and Future Electric Transportation (SeFeT)*, Aug. 2022, pp. 1–6. doi: 10.1109/SeFeT55524.2022.9908861.
- [21] Snehalika, S. Das, R. Patel, and C. K. Panigrahi, "GaN-based isolated bi-directional DC-DC converter for high load current application," in *2022 IEEE Delhi Section Conference (DELCON)*, Feb. 2022, pp. 1–7. doi: 10.1109/DELCON54057.2022.9753566.
- [22] H. Wang, Y. Zeng, S. Ji, Z. Zhao, L. Yuan, and X. Mo, "ZVS soft switching operation region analysis of modular multi active bridge converter under single phase shift control," *IEEE Transactions on Industrial Electronics*, vol. 70, no. 7, pp. 6865–6875, Jul. 2023, doi: 10.1109/TIE.2022.3204954.
- [23] S. A. Gorji, H. G. Sahebi, M. Ektesabi, and A. B. Rad, "Topologies and control schemes of bidirectional DC–DC power converters: an overview," *IEEE Access*, vol. 7, pp. 117997–118019, 2019, doi: 10.1109/ACCESS.2019.2937239.
- [24] H. Bai, Z. Nie, and C. C. Mi, "Experimental comparison of traditional phase-shift, dual-phase-shift, and model-based control of isolated bidirectional DC–DC converters," *IEEE Transactions on Power Electronics*, vol. 25, no. 6, pp. 1444–1449, Jun. 2010, doi: 10.1109/TPEL.2009.2039648.
- [25] S. Inoue and H. Akagi, "A bidirectional DC–DC converter for an energy storage system with galvanic isolation," *IEEE Transactions on Power Electronics*, vol. 22, no. 6, pp. 2299–2306, Nov. 2007, doi: 10.1109/TPEL.2007.909248.

BIOGRAPHIES OF AUTHORS






Snehalika     is assistant professor at School of Electrical Engineering, Kalinga Institute of Industrial Technology Deemed to be University, Bhubaneswar, India. She received Ph.D. degree in Electrical Engineering from KIIT Deemed to be University in 2024. She qualified GATE and received the M.Tech. degree from NIT Warangal with specialization in Power Electronics & Drives. She received the B.Tech. degree with specialization in Electronics & Electrical Engineering from KIIT Deemed to be University. Her research areas are power electronics, DC-DC converters and electric vehicle charging. She has seven years of teaching experience in education and nine years teaching experience as a GATE trainer. She can be contacted at email: snehalika.fel@kiit.ac.in.






Ranjeeta Patel     is currently an associate professor with the School of Electrical Engineering, Kalinga Institute of Industrial Technology Deemed to be University, Bhubaneswar, India. She received the Ph.D. degree in electrical engineering from the National Institute of Technology Rourkela, India, in 2017. She has more than 10 years of teaching experience. Her research interests include applications of power electronics in power quality enhancement, active power filters, grid integration and renewable energy, fuzzy controller application, and electric vehicles. She can be contacted at email: ranjeeta.patelfel@kiit.ac.in.






Amruta Abhishek    holds a bachelor of technology in Electrical Engineering from KEC, BBSR, and a master's degree in Power System Engineering from IGIT Sarang. Currently, he is pursuing his Ph.D. at KIIT in Electrical Engineering with specialization in the area of Power Electronics. He also serves as an IEEE chair member of the student branch at KIIT. His research areas are power electronics, DC-DC converters and renewable energy. He has two years of teaching experience in education. He can be contacted at email: amrutaabhishek45@gmail.com.



Chinmoy Kumar Panigrahi    is currently professor and director at School of Electrical Engineering, KIIT DU. Prof. Panigrahi's research expertise lies in the field of soft computing techniques, power systems, power electronics, renewable energy, battery management system, deregulation and smart grid. He has supervised 29 Ph.D. Scholars till date. He has published 182 research articles in referred journals and presented 148 papers in reputed conferences. He has won many accolades throughout his academic tenure of 32 years. He is also the chair for IEEE Kolkata Section Power and Energy Society-Bhubaneswar. He is a senior member of the IEEE. He is a fellow of Institution of Engineers (I). He can be contacted at email: chinmoy.panigrahifel@kiit.ac.in.



Ranjan Keshari Pati    is currently associate professor at Srinix College of Engg, Odisha, India. He received Ph.D. degree from KIIT Deemed to be University in 2014. He has more than 30 years of teaching experience. His research interests include applications of computation intelligent technique in power system problems and electric vehicles. He can be contacted at email: rkpati2014@gmail.com.